Article

Eucalyptus globulus Extract-Assisted Fabrication of Copper Oxide/Zinc Oxide Nanocomposite for Photocatalytic Applications

Muhammad Hafeez [1,*], Arooba Ghazal [1], Jahanzeb Khan [1], Pervaiz Ahmad [2], Mayeen Uddin Khandaker [3,4], Hamid Osman [5] and Sultan Alamri [5]

1   Department of Chemistry, University of Azad Jammu and Kashmir, Muzaffarabad 13100, Pakistan
2   Department of Physics, University of Azad Jammu and Kashmir, Muzaffarabad 13100, Pakistan
3   Centre for Applied Physics and Radiation Technologies, School of Engineering and Technology, Sunway University, Bandar Sunway 47500, Malaysia
4   Department of General Educational Development, Faculty of Science and Information Technology, Daffodil International University, DIU Rd, Dhaka 1341, Bangladesh
5   Department of Radiological Sciences, College of Applied Medical Sciences, Taif University, P.O. Box 2425, Taif 21944, Saudi Arabia
*   Correspondence: muhammad.hafeez@ajku.edu.pk

Abstract: In this work, we report the engineering of sub 30 nm nanoparticles of copper oxide (CuO) and Zinc oxide (ZnO) and their nanocomposite, using a green method, to degrade an organic dye (methyl orange) that is responsible for water pollution. The plant extract of *Eucalyptus globulus* was used as a capping and stabilizing agent, as it is non-toxic, easy to use, and affordable. The percent purity and composition of the samples were found using Energy Dispersive Spectroscopy (EDS), which confirmed the formation of 75% CuO nanoparticles, 77.81% ZnO nanoparticles, and 77.34% ZnO/CuO nanocomposite in respective samples. Morphological analysis was achieved using Scanning Electron Microscopy (SEM). FTIR investigations revealed that the vibrations of CuO and ZnO nanoparticles and CuO/ZnO nanocomposite were observed at 568 cm^{-1}, 617.9 cm^{-1}, and 475 cm^{-1}, respectively. The bandgap of the synthesized CuO and ZnO nanoparticles, and ZnO/CuO nanocomposite was analyzed using Diffuse Reflectance Spectroscopy (DRS), and found to be 3.36 eV, 1.83 eV, and 1.48 eV, respectively. Best photocatalytic activity confirmed that favorable conditions for the maximum degradation of methyl orange are at pH 12 and 0.02 g of the photocatalyst is required.

Keywords: CuO/ZnO nanostructures; photocatalysts; dye degradation; water remediation; green route; *Eucalyptus globulus*

1. Introduction

In the 21st century, providing clean and affordable treatment against environmental pollution is one of the biggest challenges. Environmental pollution is the gift of modernization and globalization, which is now considered a controversial issue worldwide. Industrial uprising is the need of the hour in order to meet all the essentials and comforts of life, such as food, medicines, textiles, and ceramics, etc. [1–4]. The textile industry is doing its best to uplift the economy of Asian countries, but at the same time, it is marked as a major producer of deadly pollutants in the form of organic dyes. It is estimated that about 10,000 different dyes are used industrially and 7×10^{10} dyes are produced annually worldwide, from which 10–15% of the dyes are released into industrial wastewater, as only 2–50% of the dye combines with the fabric during the dyeing process [5]. Industrial wastewater, which contains a lot of pollutants with detrimental and carcinogenic effects, is left untreated and drains into surface water resources, such as rivers and seas [6]. Apart from the aesthetics of water looking colorful and undesirable due to dye contamination, light penetration is also reduced in the water, severely affecting the photosynthetic activities of aquatic flora, which

leads to disturbances in the food chain of aquatic organisms [7]. It also reduces the amount of dissolved oxygen in the water, thereby increasing biochemical oxygen demand (BOD), which eventually damages aquatic fauna [8]. Dyes are stable organic pollutants that persist in water, and efforts have been made to degrade such pollutants, such as methyl orange, methylene blue, methylene red, and rhodamine, etc. [9,10]. As these concerns about water pollution are gaining momentum, a lot of technologies have been introduced [6], such as reverse osmosis, advanced oxidation techniques, membrane technology, and ion exchange technology [11].

Since the emergence of nanotechnology, a lot of nanomaterials have been used to degrade pollutants to protect the environment. Nanoparticles have a feature size of less than 100 nm and are used in many nanostructure devices. They are considerably smaller than the everyday objects that are governed by Newton's law of motion, but they are larger than the atoms or molecules that are subject to quantum mechanics [1,12]. They have remarkable properties, such as a large surface-to-volume ratio, solvent affinity, interfacial layers, diffusion across surfaces, ferromagnetic and ferroelectric effects, melting point depression, coating abilities, mechanical properties, and quantum mechanics effects [13]. In addition to metal oxide nanoparticles, a lot of binary metal oxides are also used as sensors, solar cells, fuel cells, and photocatalysts [14]. They have enhanced physical, chemical, optic, magnetic, electrical, flame retardancy, chemical resistance, mechanical, thermal stability, and hydrocarbon permeability properties compared to parent particles. [15] ZnO and CuO nanoparticles and ZnO/CuO nanocomposites have been used against methyl orange, due to their photocatalytic applications. ZnO metal oxide is an n-type semiconductor with a bandgap of 3.3 eV, and shows a high specific energy density as well as superior electric, optoelectronic and piezoelectric properties. CuO is a p-type semiconductor with a narrow bandgap of 1.2 eV, and has a breadth of applications in field emissions and photocatalysis [16]. Among various binary metal oxides, ZnO/CuO show fascinating properties due to their p-n characteristics, broad light absorption, and high sensitivity to humidity. As coupled semiconductors, they show two types of energy levels, which play an important role in achieving charge separation. Bandgap is reduced by coupling different types of semiconductors, which extends their absorption range to the visible region, leading to better electron–hole pair separation under irradiation, and consequently achieving superior photocatalytic activity [17,18]. Methyl orange is a mutagenic azo dye that dissolves slightly in water. It does not show a full spectrum of color changes, but shows a sharp and intense endpoint and is used as pH indicator. It is widely used in the textile industry and is resistant to complete biodegradation [19]. To fabricate these nanosized photocatalysts, green synthesis has been used, which fulfills the growing demands of ecofriendly nanomaterials due to its low-cost process rates, high energy savings and easy-to-handle process. The plant extract of *Eucalyptus globulus*, which belongs to the Myrtaceae family and is commonly known as blue gum, was used as a capping and stabilizing agent. *Eucalyptus globulus* is a popular evergreen tree used in medicines, construction, flavors, perfumes, essential oils and biopesticides [20].

Based on the above conclusions, we present this work to make a small contribution towards building a secure and ecofriendly environment. We report on an investigation into CuO and ZnO nanoparticles and their heterojunction nanocomposite as promising materials acting as photocatalysts against methyl orange. We believe these novel results are significant and will help in expanding our fundamental understanding of photocatalysis.

2. Experimental Details

2.1. Materials and Method

Zinc Sulphate ($ZnSO_4$) and Copper Sulphate ($CuSO_4$) were used as salt precursors of Zinc Oxide (ZnO) and Copper Oxide (CuO) nanoparticles and ZnO/CuO nanocomposite, which were used to perform photocatalytic activity against methyl orange. Sodium hydroxide was used to maintain the pH of the reaction mixtures. Fresh leaves of *Eucalyptus Globulus*, which were collected from the District Jhelum valley of Azad Jammu and Kashmir,

were used as a capping and stabilizing agent. All the chemicals used were of analytical grade and were purchased from Sigma Aldrich (St. Louis, MO, USA).

2.2. Preparation of Plant Extract

The collected leaves were washed with tap water and then with distilled water to remove dust particles and contamination, and were then dried in sunlight. To make the extract, 50 g of leaves were boiled in 1000 mL of distilled water at 80 °C for 3 h until the aqueous part turned into a light brown color. The liquid was cooled at room temperature and filtered using Whatman filter paper. Filtrate was poured into a measuring flask and stored in a refrigerator for further use.

2.3. Preparation of ZnO and CuO Nanoparticles

To prepare nanoparticles of Zinc and Copper oxides, 50 mL of 0.5 milimolar solution of each salt was placed in separate beakers and 20 mL of plant extract was added to both salt solutions at a constant temperature (80°) and stirring (700 rpm and 900 rpm, respectively). A total of 0.1 M Sodium hydroxide was added at regular intervals of 20 min to keep the pH at 13, in order to maintain the basic environment of the reaction mixtures. Changes in color and precipitate formation indicated the completion of the reaction, with a bright peach color for ZnO and a black color of CuO nanoparticles. Precipitates were then washed with distilled water 3–4 times to remove the anionic part of the salts and to obtain pure nanoparticles. Supernatant was removed; ZnO and CuO nanoparticles were obtained as a residue, dried at 100 °C in an oven, and converted into a fine powder using a pestle and mortar. To obtain pure and homogenized nanoparticles, calcination was performed at 350 °C for 3 h, and then again converted into fine powder.

2.4. Preparation of ZnO/CuO Nanocomposite

To prepare the nanocomposite of ZnO and CuO, precipitates were prepared separately using the above-mentioned procedure and were then mixed thoroughly by constant stirring at 700 rpm at a constant temperature of 80° for 3 h. Precipitates were allowed to settle, cooled at room temperature, and washed 3–4 times. Supernatant was discarded and ZnO/CuO nanocomposite was obtained as a residue. It was dried in an oven at 100 °C and then ground into a fine powder using a pestle and mortar. Calcination was performed at 350 °C for 3 h and then ground into homogenized fine powder.

2.5. Photocatalysis

The photocatalytic activity was carried out against methyl orange with catalyst doses of 0.2 g and 0.6 g at a pH of 7 and 12. To achieve this, the catalyst dose amounts were placed in contact with 100 mL of 10 ppm methyl orange solution and kept in the dark for half an hour to maintain adsorption–desorption equilibrium. The solutions were then analyzed using a UV spectrophotometer. After analysis, the reaction mixture was brought into sunlight with constant stirring and monitored by UV visible spectroscopy at regular intervals (0, 15, 30, 45, 60 min).

2.6. Characterization

To investigate different physiochemical properties, synthesized ZnO and CuO nanoparticles and ZnO/CuO nanocomposite were characterized using various techniques, such as FT-IR, SEM, EDS, XRD and DRS. The chemical composition of the prepared samples was analyzed with the help of an FTIR spectrophotometer (Shimazdu 8400S, Thermo Fisher Scientific, Waltham, MA, USA), in the range of 400–4000 cm^{-1}. Morphology was investigated using a scanning electron microscope (Nova nano SEM, Model 450, Manufacturer: FEI, Hillsboro, OR, USA), and EDS was used for the elemental analysis of the samples. XRD was used to analyze crystalline structure and crystal phases of the samples. DRS was used for the determination of different components of a sample.

3. Results and Discussion

### 3.1. Characterization of Synthesized Materials

Figure 1 shows the results of analyses performed to confirm the formation of ZnO and CuO NPs and ZnO/CuO nanocomposite. The results give the percentage elemental composition of the constituents present in each sample.
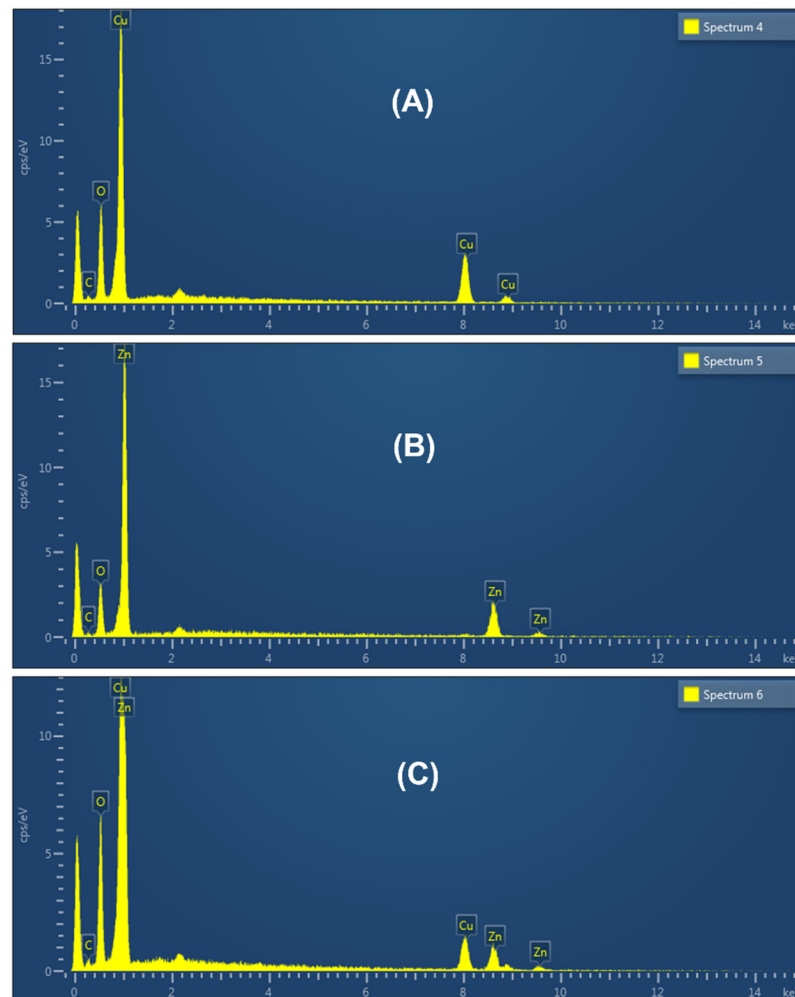
Figure 1. EDS results of (**A**) ZnO, (**B**) CuO Nps and (**C**) ZnO/CuO nanocomposite.

Figure 1A confirmed the formation of ZnO NPs containing Zn and O, with weight percentages of 77, 81 and 19%, respectively. Figure 1B revealed the presence of Cu and O, with weight percentages of 75.13 and 21.68%, respectively. In Figure 1C, ZnO/CuO nanocomposite was confirmed as containing 43.81, 33.53, 19.75%, Zn, Cu and O, respectively. Traces of carbon were also seen in these three spectrums as the sample was prepared by green synthesis, using *Eucalyptus globulus* as the stabilizing agent.

The results of morphological studies of the ZnO and CuO nanoparticles and ZnO/CuO nanocomposite are shown in Figure 2, and were carried out using a Nova Nano Scanning Emission Spectroscopy (SEM) at the magnification of 500 nm. Figure 2A shows the formation of ZnO nanoparticles, and it is obvious that these particles are nanosized, since the particles were calcined at 300 °C, so agglomeration is due to hydrolysis. Nucleation rate and growth rate are rapid due to the higher temperatures, so dense and thick particles with a wide size distribution are seen. The micrograph shows that the individual ZnO nanoparticles show irregular shapes with clear boundaries. M. Sundrarajanet.al synthesized ZnO nanoparticles, and SEM images gave an average size of 100 nm, with agglomeration and cavities at some points [21].
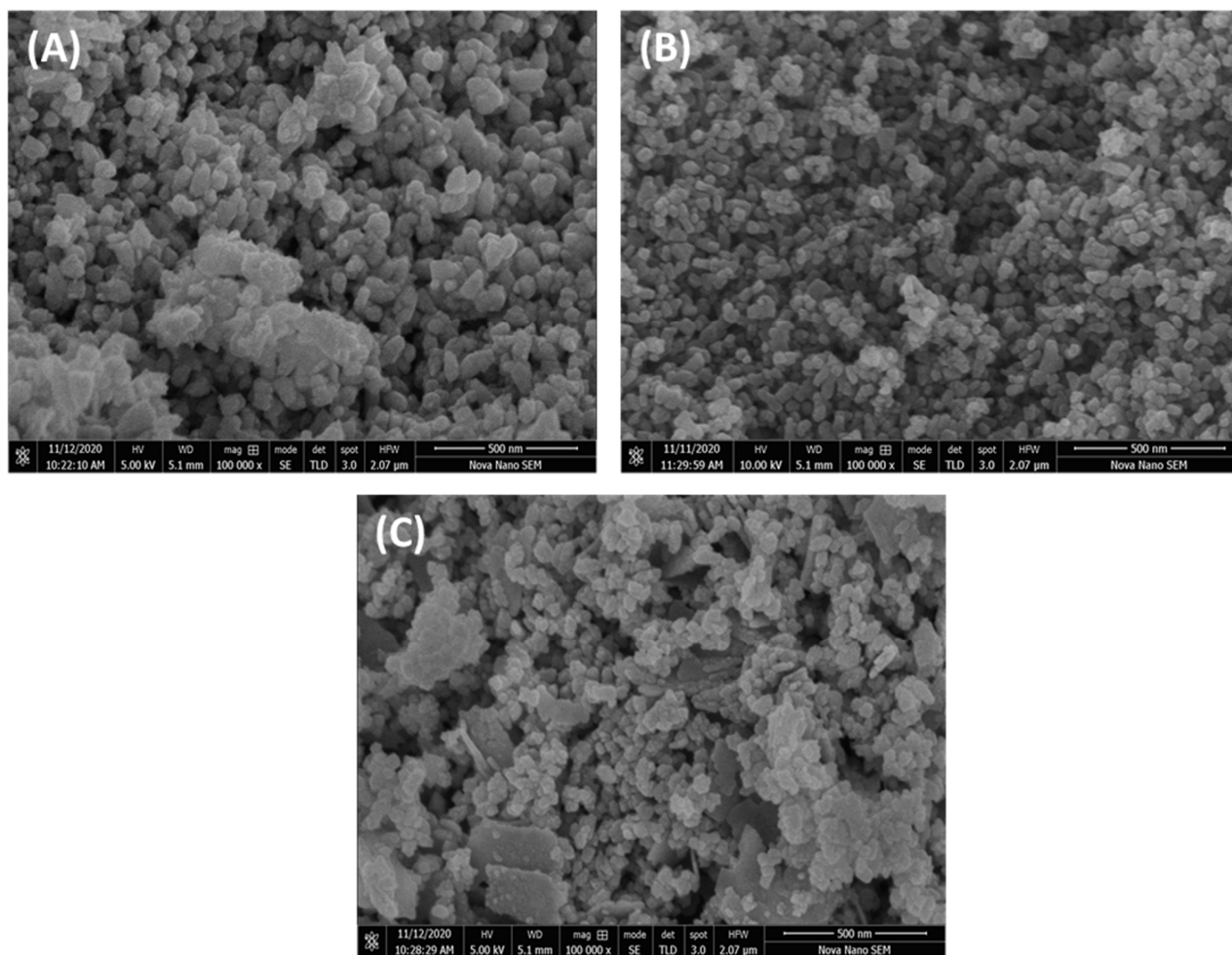
Figure 2. SEM micrographs of (**A**) ZnO, (**B**) CuO nanoparticles and (**C**) ZnO/CuO nanocomposite.

Figure 2B shows a micrograph of CuO nanoparticles that were also calcined at 300 °C, but gave a different effect. The agglomerated part was turned into even smaller-sized nanoparticles at the same temperature. The micrograph represents nanoparticles with a near-regular and spherical shape. The nucleation and growth rate of the sample are high and give a wide size distribution. D. Vaidehi synthesized CuO nanoparticles by green synthesis and reported the shapes to be near-spherical, with size ranges between 20 and 40 nm [22]. Figure 2C represents the combination of ZnO and CuO nanoparticles in the form of a nanocomposite, where spherical CuO nanoparticles are seen on the surface of agglomerated ZnO nanoparticle chunks, increasing its surface area with cavities at some points. R. Saravanan et al. synthesized ZnO/CuO nanocomposite with an average size of 35 nm [23].

In the reported work, sizes of ZnO and CuO nanoparticles and ZnO/CuO nanocomposite are estimated to be 55.41 nm, 36.28 nm and 39.19 nm, respectively. The size of the ZnO/CuO nanocomposite is a little higher then CuO nanoparticles due to the agglomerated part of the ZnO nanoparticles. Figure 3A–C show the FTIR spectra for the ZnO and CuO nanoparticles and ZnO/CuO nanocomposite, respectively. The spectra possess a broad stretching peak at 3200–3600 cm^{-1} which is attributed to the O-H bond, possibly from H_2O molecules [23]. A sharp set of peaks in the range of 1550–1750 cm^{-1} are ascribed to the stretching vibrations of C=O, and peaks at 1545 cm^{-1} are taken as absorption peaks of an M-O bond [24]. Another peak at 1446.5 cm^{-1} is only seen in the spectra of the ZnO/CuO nanocomposite and is attributed to C=O that remains adsorbed on the surface of the ZnO/CuO nanocomposite. A very fine peak at 1396 cm^{-1} is ascribed to the

deformation vibration of alkene C-H bonds. Peaks in the range of 1000–1200 cm^{-1} are attributed to M-O bond formations in the presence of the NaOH, which was used as the nanomaterial synthesis base [25]. Stretching vibrations of aromatic C-H bonds are seen, and are due to the use of plant material as a stabilizing agent in the synthesis. Strong absorptive peaks are seen in the range of 500–700 cm^{-1} and are attributed to the M-O bond in either ZnO or CuO.
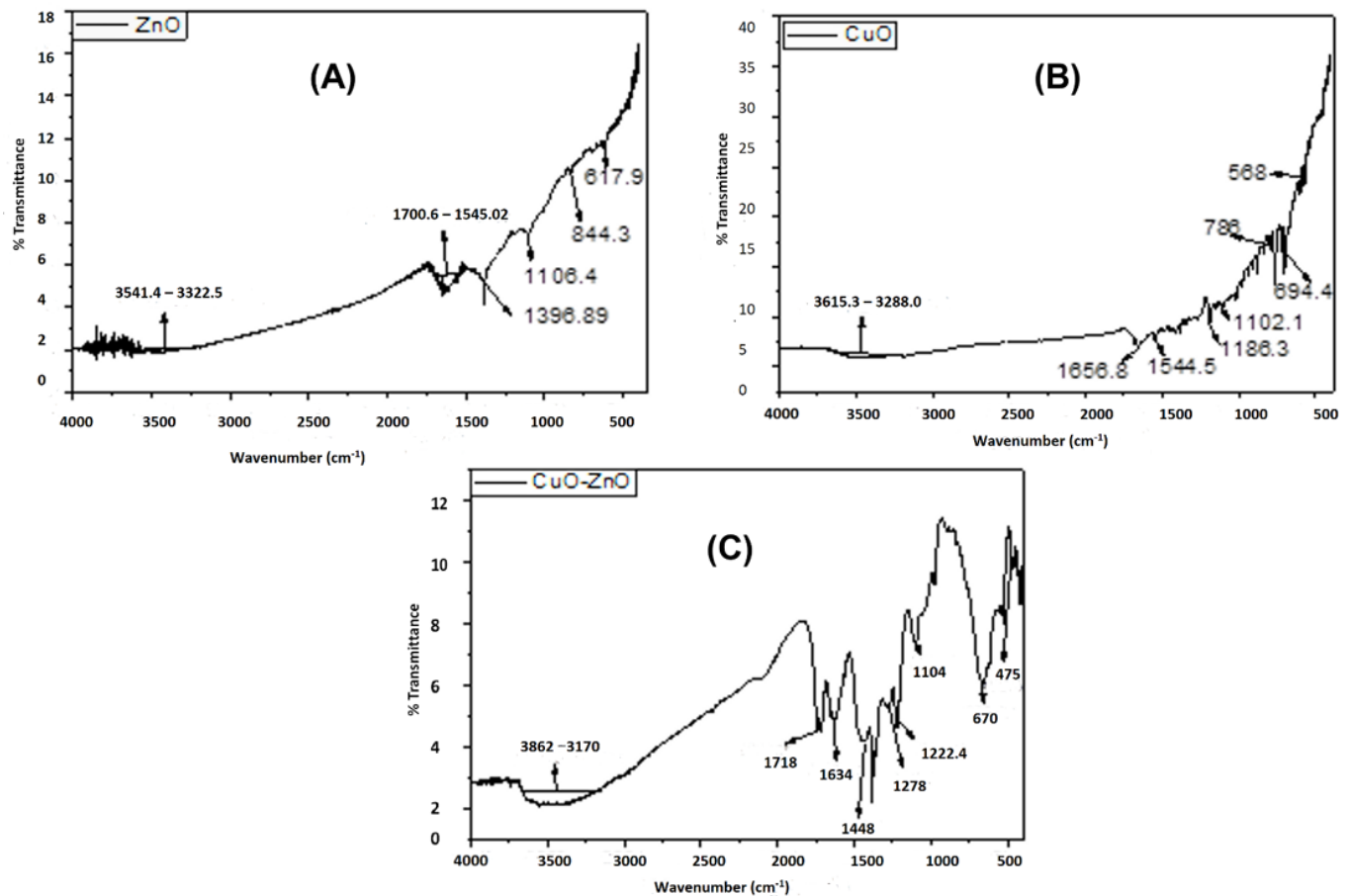
Figure 3. (**A**) FTIR spectra of ZnO, (**B**) CuO Nps and (**C**) ZnO/CuO nanocomposite.

This is the confirmation peak for the synthesis of the M-O bond. Zn-O stretching vibrations are shifted from 617 cm^{-1} to 670 cm^{-1}, with the addition of Cu-O in the spectra of ZnO/CuO nanocomposite. The peak at 475 cm^{-1} is attributed to the stretching mode of a combination of Zn-O and Cu-O nanoparticles [24]. The diffuse reflectance spectra of synthesized ZnO and CuO nanoparticles and ZnO/CuO nanocomposite are given in Figure 4A–C, respectively. It is shown that with the gradual increase in wavelength and the spectra changing from ultraviolet to the visible range, transmittance is increased, and a clear red shift is observed. Here, the wavelength of transmittance edge was determined by extrapolating the sharply rising and horizontal part of the curve which is between 600 and 700 nm. The bandgap of the ZnO and CuO nanoparticles and ZnO/CuO nanocomposite were calculated to be 3.36 eV, 1.83 eV and 1.48 eV, respectively. From the spectra, it can be seen that the bandgap of the ZnO/CuO nanocomposite is less than that of corresponding nanoparticles, which could be explained by quantum confinement effects.
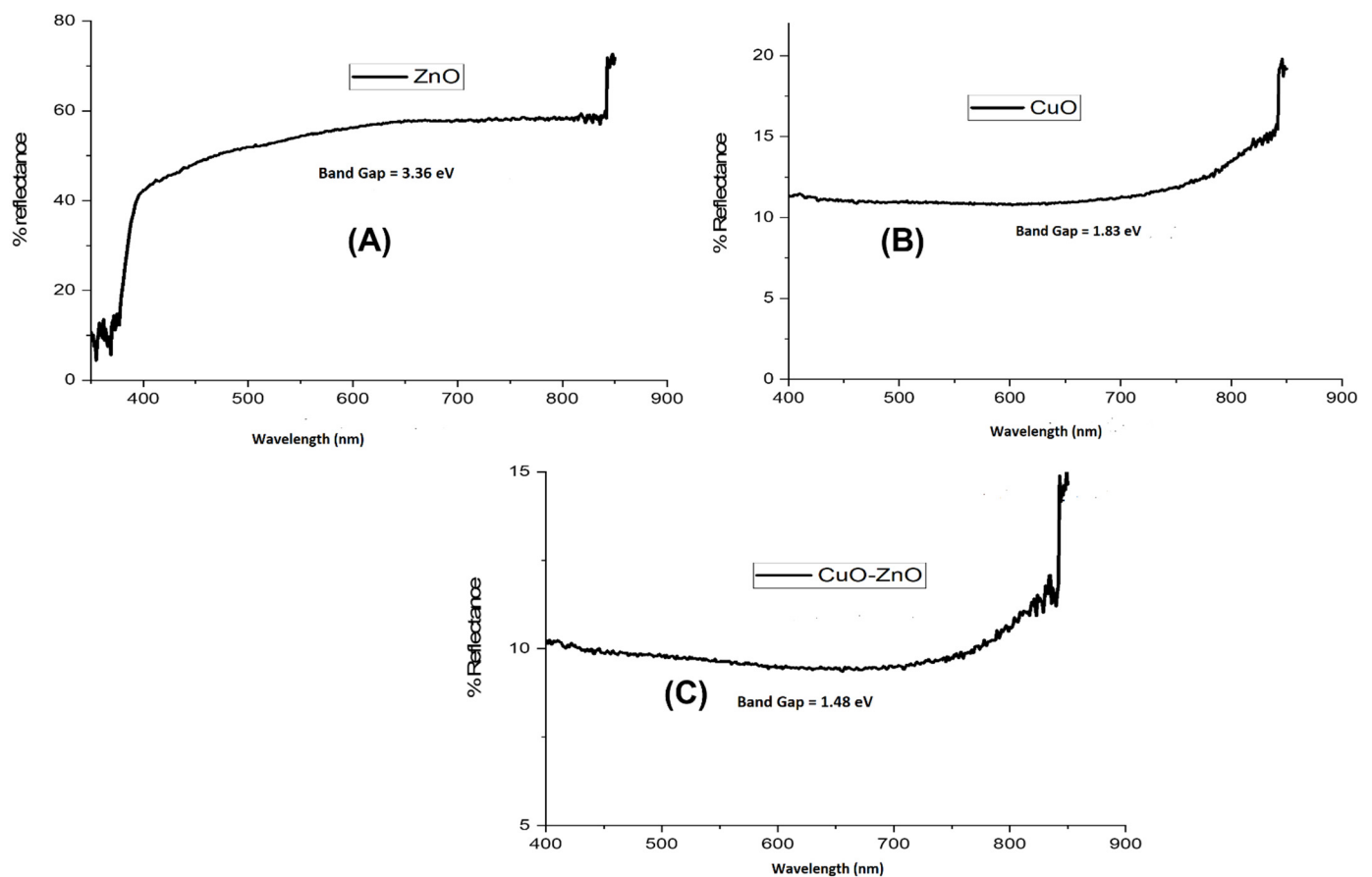
Figure 4. DRS spectra of (**A**) ZnO, (**B**) CuO Nps and (**C**) ZnO/CuO nanocomposite.

The X-ray diffractograms of the CuO and ZnO nanoparticles and CuO/ZnO nanocomposite are given in Figure 5A–C, respectively. The X-ray diffractogram of the ZnO nanoparticles possesses diffraction peaks, along with the miller planes in parenthesis, being 31.88(100), 34.74(002), 36.51(101), 47.79(102), 56.77(110), 63.02(103), 68.06(112), 69.42(201), 72.68(004) and 77.03(202), corresponding to reference card no. 01-075-0576. The calculated crystallite size for the hexagonal-shaped crystallite is 28.30 nm, with 0.391% lattice strain found in the crystal. The diffractogram of the CuO nanoparticles possesses sharp peaks at 32.70, 35.66, 38.91, 48.85, 53.79, 58.54, 61.81, 66.29, 68.19 and 75.38, which are due to the (110), (−111), (111), (−202), (020), (−113), (−311), (−221) and (−222) miller planes, respectively. These data were found to be the same as those reported in reference card no. 01-072-0629, confirming the formation of monoclinic-shaped crystallites. The crystallite size, calculated from the most intense diffraction peak, is 42.8 nm, with 0.244% lattice strain in the crystal. The CuO/ZnO diffractogram shows two separate sets of diffraction peaks for CuO and ZnO nanoparticles. The peaks for CuO appeared at 35.83, 38.82 and 58.40, due to the diffraction of X-ray from the (−111), (111) and (202) miller planes, respectively. The monoclinic shape of the crystallites, with a size of 34.20 nm, was confirmed by reference card no. 01-080-1268. A 0.304% lattice strain was found in the crystal. The diffraction peaks, along with the miller planes for ZnO, were seen at 31.88(100), 34.74(002), 36.51(101), 47.79(102), 56.77(110), 63.02(103), 66.43(200), 68.06(112), 69.42(201) and 72.68(004). The data matched with reference card no. 01-075-0576, confirming the formation of hexagonal shape crystallites with a size of 28.30 nm.
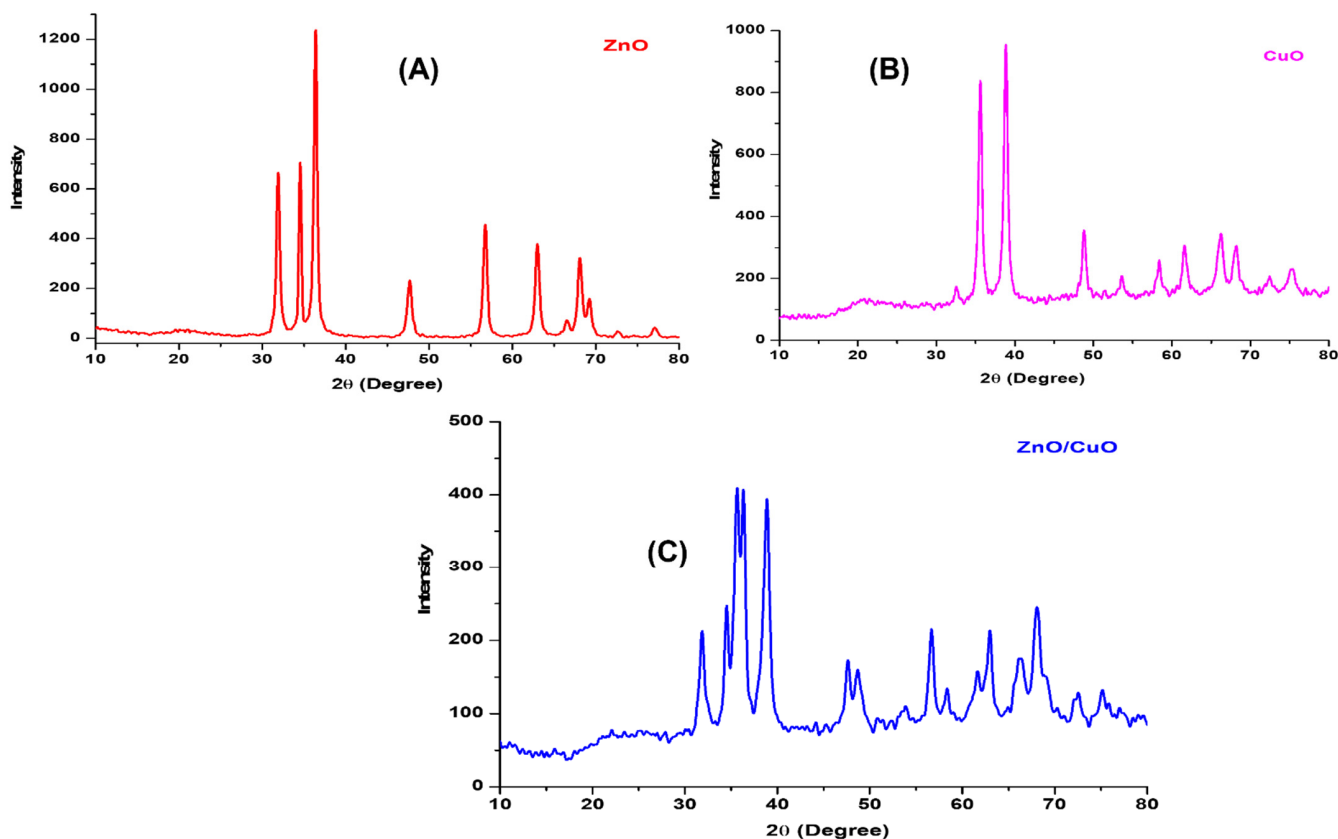
Figure 5. XRD spectra of (**A**) ZnO, (**B**) CuO Nps and (**C**) ZnO/CuO nanocomposite.

3.2. Photocatalytic Activity

The photocatalytic activity of ZnO and CuO nanoparticles and ZnO/CuO nanocomposite, which were synthesized by a green method, was investigated against methyl orange under sunlight for 90 min (30 min in dark, 60 min in sunlight). Maximum absorbance of methyl orange is seen at 464 nm, and the reaction was spectrophotometrically monitored at regular intervals, showing a reduction in absorption maxima as a function of time (0, 15, 30, 45, 60 shown in Figure 6A). The percentage degradation of the methyl orange was calculated using the following formula.

$$\%D = \frac{C_t - C_o}{C_o} \times 100 \tag{1}$$

where C_o is the initial concentration of the dye before irradiation and C_t is the concentration of the dye at a specific reaction time, t, after irradiation [26].

The formation of the p-n heterojunction, by the combination of ZnO and CuO, enhanced the photocatalytic efficiency of the ZnO nanoparticles. The bandgap of ZnO and CuO is 3.36 and 1.83 eV, with electron affinities of 4.35 and 4.07 eV, respectively [17]. It is anticipated that photons of visible light energy excite the valence electrons of CuO because of its small bandgap energy, leaving a hole in the valence band of CuO which migrate towards ZnO, performing reduction reactions, and generating superoxide ions. Moreover, electron decay from the conduction band of ZnO to the valence band of CuO is nearly impossible, so the hole acts to facilitate oxidation reactions with the formation of OH and H_2O_2 species, which have a high degradation efficiency against organic pollutants [16].

A classical Tauc approach was used to find the energy bandgap of the prepared nanocrystals. (Shown in Figure 6B) The following equation was used to estimate the energy bandgap of the titanium oxide crystallites.
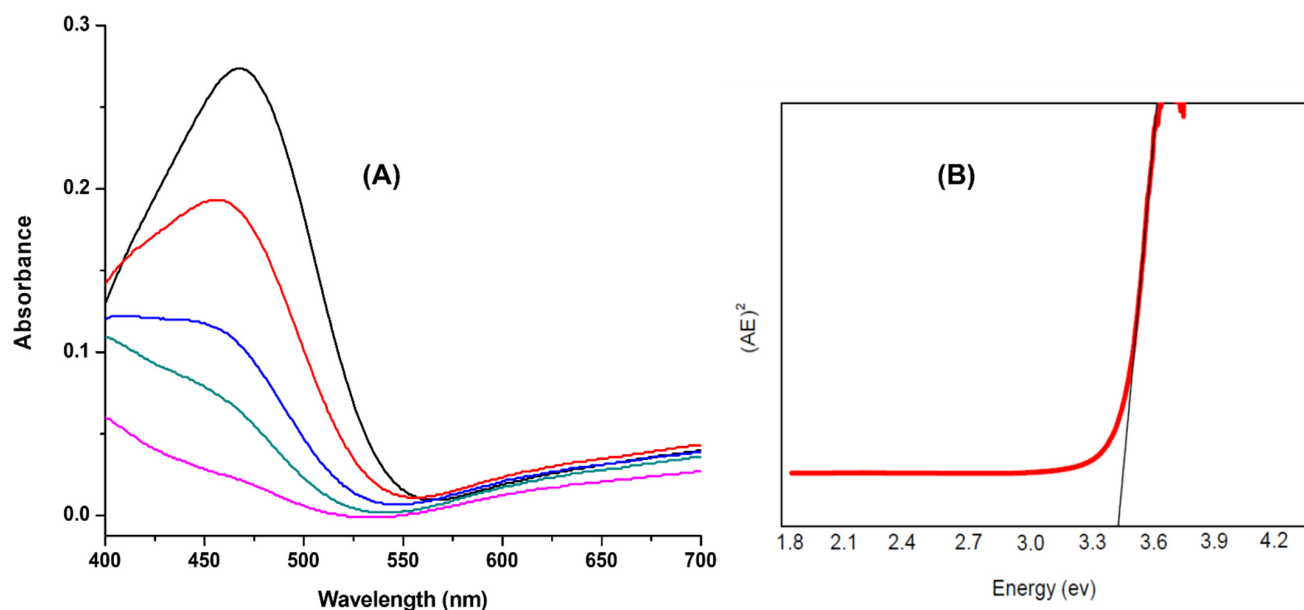
Figure 6. (**A**) Photocatalytic activity performance measures for ZnO/CuO nanocomposite, as a function of time (0, 15, 30, 45, 60) min (from pink to black line, respectively). (**B**) Corresponding Tauc plot for bandgap calculation.

$$\alpha h\nu = K(h\nu - E_g)^n$$

where $h\nu$ is the incident photon energy, α indicates the absorption coefficient, E_g refers to the optical bandgap, K, and is a proportionality constant, and h refers to the Planck constant. The exponential, n, depends on the type of band-band transition; it is 2 for a direct bandgap and 1/2 for an indirect bandgap. The bandgap estimated from the Tauc plot is 3.35 eV greater than that of the bulk, showing the successful synthesis of nano-sized material [27]. Thus, the heterojunction formed by the combination of ZnO and CuO acts to prevent recombination of photo-generated pairs, which allows for superior oxidative species generation. The whole mechanism is illustrated below in Figure 6B. The introduction of NH2-MIL-125(Ti) into the hybrid materials could modulate their optical, electronic and redox properties, and promote the charge separation, owing to the formation of the heterojunction, thus resulting in an enhanced photocatalytic performance for organic pollutant decomposition. As such, the NH2-MIL-125(Ti)/TTB-TTA composite has a much higher photodegradation kinetic of methyl orange (MO), which is over 9 and 2 times the rates of pure NH2-MIL-125(Ti) and TTB-TTA, respectively. This versatile molecular-material platform can achieve dual adjusting modes consisting of a COF molecular engineering and an MOF-type screening strategy, which will be applicable to a wide range of fields [28,29].

3.3. Effect of Concentration of Photocatalyst

The effect of catalyst loading was observed by varying the photocatalyst mass from 0.02 g to 0.06 g for the photodegradation of methyl orange. This showed that the percent degradation of methyl orange by ZnO nanoparticles and ZnO/CuO nanocomposite is higher at 0.02 g and decreases as the catalyst dose increases to 0.06 g, as shown in Figure 7A–D. The % degradation of methyl orange by ZnO at 0.02 and 0.06 g is 32% and 7%, respectively, while the photocatalytic efficiency of ZnO/CuO nanocomposite is 65% and 9%, respectively.
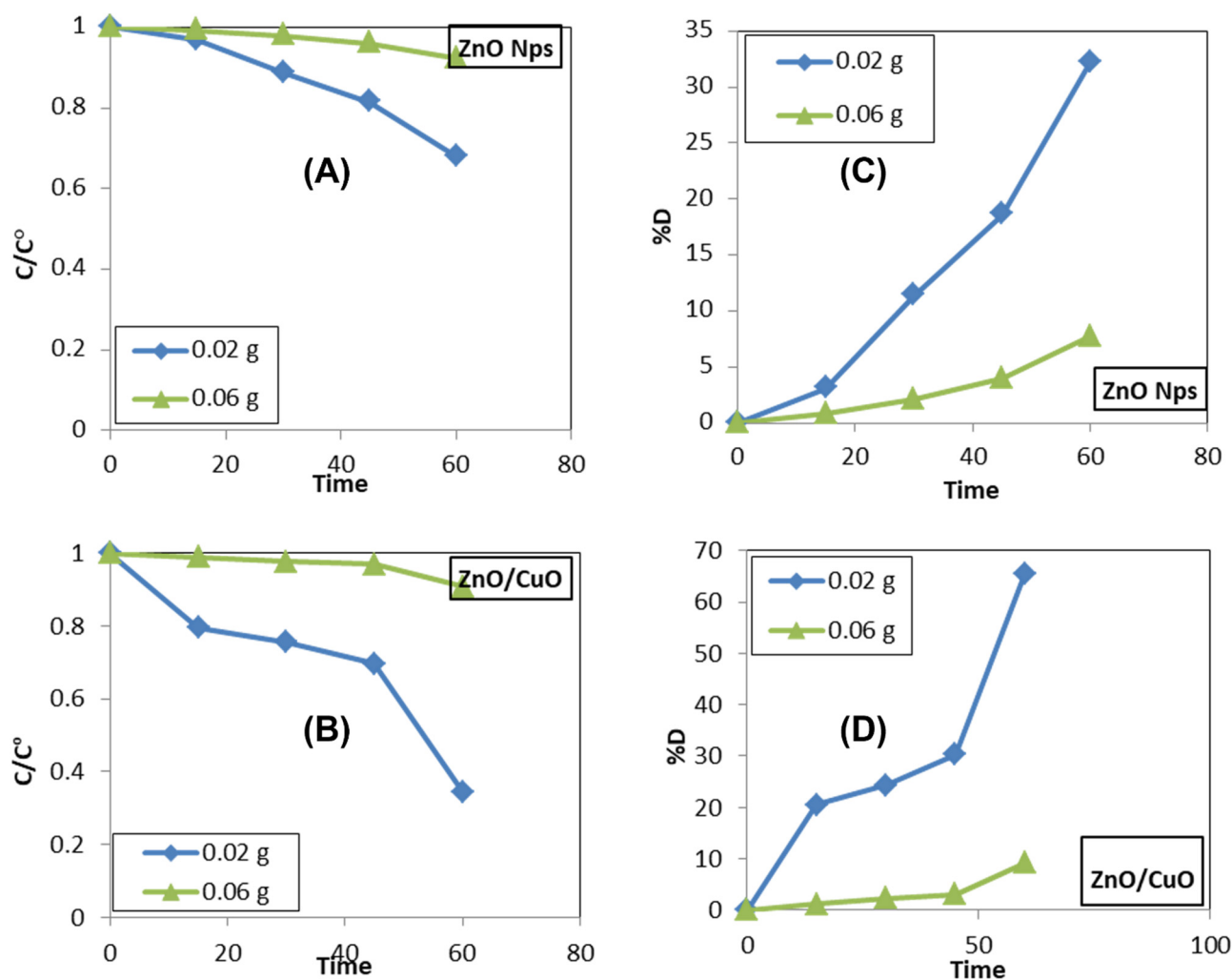
Figure 7. (**A**,**B**) C/Co of ZnO Nps and ZnO/CuO nanocomposite at 0.02 g and 0.06 g, and (**C**,**D**) % degradation of ZnO Nps and ZnO/CuO nanocomposite at 0.02 g and 0.06 g.

Conversely, by adding CuO to ZnO, the photocatalytic degradation of methyl orange is enhanced due to the formation of the p-n junction. ZnO nanoparticles provide 32% degradation while ZnO/CuO nanocomposite provides 65% degradation at a concentration of 0.02 g. With the increase in catalyst mass from 0.02 to 0.06 g, more hydroxyl and superoxide radicals are generated.

As the dye concentration is fixed, an increase in catalyst concentration causes aggregation of the catalyst, which decreases the surface area that is available for the photodegradation of methyl orange to take place. Another reason for the decrease in photodegradation with the increase in catalyst dose, is that the reaction mixture becomes turbid and cloudy, which affects the light penetration required for the photodegradation process, since the photocatalyst absorbs less light [30–32].

3.4. Effect of pH

To study the effect of pH, initial concentrations of the reaction mixture were adjusted to a desired pH by adding 1.0 M NaOH as a base. In the plot of C/Co vs. time, a gradual decrease in absorbance could be seen, which indicates the degradation of the dye [33].

It is shown in Figure 8A–D that the percentage degradation of methyl orange is low at a neutral pH, but sharply increases by increasing the pH. The % degradation of methyl orange by ZnO nanoparticles is 32% and 91%, but is 65% and 85% for the ZnO/CuO nanocomposite. The increase in photodegradation of methyl orange with the increase in

pH could be explained by the acid-base behavior of the photocatalyst. By increasing the pH, more hydroxyl radicals are generated that take part in the photodegradation of the dye, in addition to the hydroxyl and superoxide ions generated by the photocatalyst.
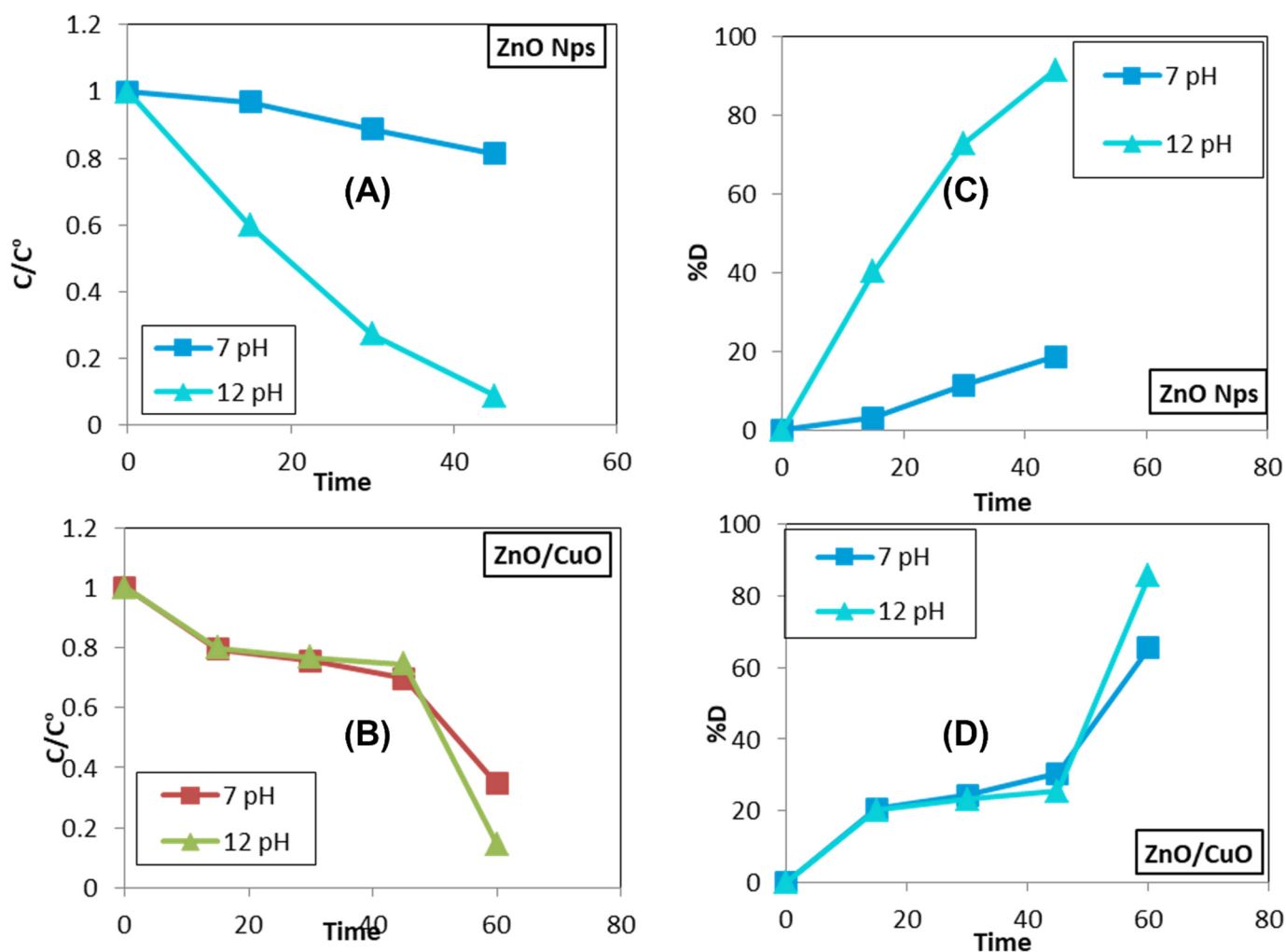
Figure 8. (**A**,**B**) C/Co of ZnO Nps and ZnO/CuO nanocomposite at pH 7 &12, and (**C**,**D**) % degradation of ZnO Nps and ZnO/CuO nanocomposite at pH 7 &12.

4. Conclusions

In summary, it has been proved that a green method is a very easy, affordable and inexpensive way to synthesize nanomaterials. Using this green method, the engineering of sub 30 nm nanoparticles of Copper oxide (CuO), Zinc oxide (ZnO), and their nanocomposite to degrade organic dye (methyl orange), responsible for water pollution, has been successfully formulated and reported. The plant extract of *Eucalyptus globulus* was used as a capping and stabilizing agent as it is non-toxic, easy to use, and affordable. The synthesized ZnO and CuO nanoparticles and their nanocomposite were characterized using various techniques, such as FT-IR, SEM, EDS, XRD and DRS. All the results validate each other. The efficiency of ZnO nanoparticles is enhanced by adding CuO, and the formation of p-n junction and the enhanced photocatalytic activity could be attributed to the morphology and surface area of the photocatalyst. The best photocatalytic activity confirmed that favorable conditions for the maximum degradation of methyl orange are at pH 12, and only 0.02 g of the photocatalyst is required. We believe that these novel results are significant and will pave the way to expand our fundamental understanding of photocatalysis.

References

1. Ahmed, S.; Jiang, X.; Wang, C.; Kalsoom, U.E.; Wang, B.; Khan, J.; Muhammad, Y.; Duan, Y.; Zhu, H.; Ren, X.; et al. An Insightful Picture of Nonlinear Photonics in 2D Materials and their Applications: Recent Advances and Future Prospects. *Adv. Opt. Mater.* **2021**, *9*, 2001671. [CrossRef]
2. Cook, T.R.; Zheng, Y.R.; Stang, P.J. Metal-organic frameworks and self-assembled supramolecular coordination complexes: Comparing and contrasting the design, synthesis, and functionality of metal-organic materials. *Chem. Rev.* **2013**, *113*, 734–777. [CrossRef] [PubMed]
3. Ding, M.; Flaig, R.W.; Jiang, H.L.; Yaghi, O.M. Carbon capture and conversion using metal-organic frameworks and MOF-based materials. *Chem. Soc. Rev.* **2019**, *48*, 2783–2828. [CrossRef]
4. Belmabkhout, Y.; Bhatt, P.M.; Adil, K.; Pillai, R.S.; Cadiau, A.; Shkurenko, A.; Maurin, G.; Liu, G.; Koros, W.J.; Eddaoudi, M. Natural gas upgrading using a fluorinated MOF with tuned H_2S and CO_2 adsorption selectivity. *Nat. Energy* **2018**, *3*, 1059–1066. [CrossRef]
5. Pereira, L.; Alves, M. Dyes—Environmental impact and remediation. In *Environmental Protection Strategies for Sustainable Development*; Springer: Berlin/Heidelberg, Germany, 2012; pp. 111–162.
6. Hayder, R.; Hafeez, M.; Zaheer, M. Challenges for sustainable water use in the northern part of Pakistan focusing on hydrology assessment of non-industrial zone. *J. Clean. Prod.* **2022**, *349*, 131166. [CrossRef]
7. Mekonnen, M.M.; Hoekstra, A.Y. Global gray water footprint and water pollution levels related to anthropogenic nitrogen loads to fresh water. *Environ. Sci. Technol.* **2015**, *49*, 12860–12868. [CrossRef]
8. Malik, D.S.; Sharma, A.K.; Sharma, A.K.; Thakur, R.; Sharma, M. A review on impact of water pollution on freshwater fish species and their aquatic environment. *Adv. Environ. Pollut. Manag. Wastewater Impacts Treat. Technol.* **2020**, *1*, 10–28.
9. Shanker, U.; Rani, M.; Jassal, V. Degradation of hazardous organic dyes in water by nanomaterials. *Environ. Chem. Lett.* **2017**, *15*, 623–642. [CrossRef]
10. Khan, J.; Ilyas, S.; Akram, B.; Ahmad, K.; Hafeez, M.; Siddiq, M.; Ashraf, M.A. Zno/NiO coated multi-walled carbon nanotubes for textile dyes degradation. *Arab. J. Chem.* **2018**, *11*, 880–896. [CrossRef]
11. Khatun, R. Water pollution: Causes, consequences, prevention method and role of WBPHED with special reference from Murshidabad District. *Int. J. Sci. Res. Publ.* **2017**, *7*, 269–2250.
12. Bhushan, B. Introduction to nanotechnology. In *Springer handbook of Nanotechnology*; Springer: Berlin/Heidelberg, Germany, 2017; pp. 1–19.
13. Rao, C.N.R.; Müller, A.; Cheetham, A.K. *The Chemistry of Nanomaterials: Synthesis, Properties and Applications*; John Wiley & Sons: Hoboken, NJ, USA, 2006.
14. Fu, X.; Clark, L.A.; Yang, Q.; Anderson, M.A. Enhanced photocatalytic performance of titania-based binary metal oxides: TiO_2/SiO_2 and TiO_2/ZrO_2. *Environ. Sci. Technol.* **1996**, *30*, 647–653. [CrossRef]
15. Magdalane, C.M.; Kaviyarasu, K.; Matinise, N.; Mayedwa, N.; Mongwaketsi, N.; Letsholathebe, D.; Mola, G.; AbdullahAl-Dhabi, N.; Arasu, M.V.; Henini, M.; et al. Evaluation on La_2O_3 garlanded ceria heterostructured binary metal oxide nanoplates for UV/visible light induced removal of organic dye from urban wastewater. *S. Afr. J. Chem. Eng.* **2018**, *26*, 49–60. [CrossRef]
16. Oliveira, M.; Fonseca, V.; Neto, N.A.; Ribeiro, R.; Longo, E.; de Lazaro, S.; Motta, F.; Bomio, M. Connecting theory with experiment to understand the photocatalytic activity of CuO–ZnO heterostructure. *Ceram. Int.* **2020**, *46*, 9446–9454. [CrossRef]
17. Harish, S.; Archana, J.; Sabarinathan, M.; Navaneethan, M.; Nisha, K.; Ponnusamy, S.; Muthamizhchelvan, C.; Ikeda, H.; Aswal, D.; Hayakawa, Y. Controlled structural and compositional characteristic of visible light active ZnO/CuO photocatalyst for the degradation of organic pollutant. *Appl. Surf. Sci.* **2017**, *418*, 103–112. [CrossRef]
18. Khan, J.; Siddiq, M.; Akram, B.; Ashraf, M.A. In-situ synthesis of CuO nanoparticles in P(NIPAM-co-AAA) microgel, structural characterization, catalytic and biological applications. *Arab. J. Chem.* **2018**, *11*, 897–909. [CrossRef]

19. Jiang, L.; Yuan, X.; Zeng, G.; Chen, X.; Wu, Z.; Liang, J.; Zhang, J.; Wang, H.; Wang, H. Phosphorus-and sulfur-codoped g-C3N4: Facile preparation, mechanism insight, and application as efficient photocatalyst for tetracycline and methyl orange degradation under visible light irradiation. *ACS Sustain. Chem. Eng.* **2017**, *5*, 5831–5841. [CrossRef]

20. Bean, C.; Russo, M.J.J.T.N.C. Element Stewardship Abstract for *Eucalyptus globulus*. Available online: http://www.invasive.org/gist/esadocs/documnts/eucaglo.pdf (accessed on 1 June 2020).

21. Sundrarajan, M.; Ambika, S.; Bharathi, K. Plant-extract mediated synthesis of ZnO nanoparticles using Pongamia pinnata and their activity against pathogenic bacteria. *Adv. Powder Technol.* **2015**, *26*, 1294–1299. [CrossRef]

22. Vaidehi, D.; Bhuvaneshwari, V.; Bharathi, D.; Sheetal, B.P. Antibacterial and photocatalytic activity of copper oxide nanoparticles synthesized using Solanum lycopersicum leaf extract. *Mater. Res. Express* **2018**, *5*, 085403. [CrossRef]

23. Saravanan, R.; Karthikeyan, S.; Gupta, V.; Sekaran, G.; Narayanan, V.; Stephen, A. Enhanced photocatalytic activity of ZnO/CuO nanocomposite for the degradation of textile dye on visible light illumination. *Mater. Sci. Eng. C* **2013**, *33*, 91–98. [CrossRef]

24. Widiarti, N.; Sae, J.; Wahyuni, S. Synthesis CuO-ZnO nanocomposite and its application as an antibacterial agent. In Proceedings of the IOP Conference Series: Materials Science and Engineering, Busan, Korea, 25–27 August 2017; p. 012036.

25. Singh, P.K.; Kumar, P.; Hussain, M.; DAS, A.K.; Nayak, G.C. Synthesis and characterization of CuO nanoparticles using strong base electrolyte through electrochemical discharge process. *Bull. Mater. Sci.* **2016**, *39*, 469–478. [CrossRef]

26. Zeid, E.A.; Ibrahem, I.A.; Mohamed, W.A.; Ali, A.M. Study the influence of silver and cobalt on the photocatalytic activity of copper oxide nanoparticles for the degradation of methyl orange and real wastewater dyes. *Mater. Res. Express* **2020**, *7*, 026201. [CrossRef]

27. Reddy, K.M.; Manorama, S.V.; Reddy, A.R. Bandgap studies on anatase titanium dioxide nanoparticles. *Mater. Chem. Phys.* **2003**, *78*, 239–245. [CrossRef]

28. Zhu, Y.; Liu, Y.; Ai, Q.; Gao, G.; Yuan, L.; Fang, Q.; Tian, X.; Zhang, X.; Egap, E.; Ajayan, P.M.; et al. In Situ Synthesis of Lead-Free Halide Perovskite–COF Nanocomposites as Photocatalysts for Photoinduced Polymerization in Both Organic and Aqueous Phases. *ACS Mater. Lett.* **2022**, *4*, 464–471. [CrossRef]

29. He, S.; Rong, Q.; Niu, H.; Cai, Y. Platform for molecular-material dual regulation: A direct Z-scheme MOF/COF heterojunction with enhanced visible-light photocatalytic activity. *Appl. Catal. B: Environ.* **2019**, *247*, 39–56. [CrossRef]

30. Jefri, S.N.S.; Abdullah, A.H.; Muhamad, E.N. Response surface methodology: Photodegradation of methyl orange by CuO/ZnO under UV light irradiation. *Asian J. Green Chem.* **2019**, *3*, 271–287.

31. Akram, B.; Ahmad, K.; Khan, J.; Khan, B.A.; Akhtar, J. Low-temperature solution-phase route to sub-10 nm titanium oxide nanocrystals having super-enhanced photoreactivity. *New J. Chem.* **2018**, *42*, 10947–10952. [CrossRef]

32. Lustig, W.P.; Mukherjee, S.; Rudd, N.D.; Desai, A.V.; Li, J.; Ghosh, S.K. Metal-organic frameworks: Functional luminescent and photonic materials for sensing applications. *Chem. Soc. Rev.* **2017**, *46*, 3242–3285. [CrossRef]

33. Chiu, Y.-H.; Chang, T.-F.M.; Chen, C.-Y.; Sone, M.; Hsu, Y.-J. Mechanistic Insights into Photodegradation of Organic Dyes Using Heterostructure Photocatalysts. *Catalysts* **2019**, *9*, 430. [CrossRef]